

Version 2.2 as of March 13, 2011

Contact persons: Marc Besançon, Frédéric Déliot, Cécile Deterre

Alexander Grohsjean, Yvonne Peters, Elizaveta Shabalina, Slava Sharyy

To be submitted to PLB

Comment to d0-run2eb-010@fnal.gov

by XX FNAL time

DØ INTERNAL DOCUMENT – NOT FOR PUBLIC DISTRIBUTION

author list dated 17 February 2011

1 **Measurement of the $t\bar{t}$ production cross section using dilepton events in $p\bar{p}$ collisions**

2 V.M. Abazov,³⁵ B. Abbott,⁷³ B.S. Acharya,²⁹ M. Adams,⁴⁹ T. Adams,⁴⁷ G.D. Alexeev,³⁵ G. Alkhalaf,³⁹
3 A. Alton^a,⁶¹ G. Alverson,⁶⁰ G.A. Alves,² L.S. Ancu,³⁴ M. Aoki,⁴⁸ M. Arov,⁵⁸ A. Askew,⁴⁷ B. Åsman,⁴¹
4 O. Atramentov,⁶⁵ C. Avila,⁸ J. BackusMayes,⁸⁰ F. Badaud,¹³ L. Bagby,⁴⁸ B. Baldin,⁴⁸ D.V. Bandurin,⁴⁷
5 S. Banerjee,²⁹ E. Barberis,⁶⁰ P. Baringer,⁵⁶ J. Barreto,³ J.F. Bartlett,⁴⁸ U. Bassler,¹⁸ V. Bazterra,⁴⁹ S. Beale,⁶
6 A. Bean,⁵⁶ M. Begalli,³ M. Begel,⁷¹ C. Belanger-Champagne,⁴¹ L. Bellantoni,⁴⁸ S.B. Beri,²⁷ G. Bernardi,¹⁷
7 R. Bernhard,²² I. Bertram,⁴² M. Besançon,¹⁸ R. Beuselinck,⁴³ V.A. Bezzubov,³⁸ P.C. Bhat,⁴⁸ V. Bhatnagar,²⁷
8 G. Blazey,⁵⁰ S. Blessing,⁴⁷ K. Bloom,⁶⁴ A. Boehnlein,⁴⁸ D. Boline,⁷⁰ T.A. Bolton,⁵⁷ E.E. Boos,³⁷ G. Borissov,⁴²
9 T. Bose,⁵⁹ A. Brandt,⁷⁶ O. Brandt,²³ R. Brock,⁶² G. Brooijmans,⁶⁸ A. Bross,⁴⁸ D. Brown,¹⁷ J. Brown,¹⁷ X.B. Bu,⁴⁸
10 M. Buehler,⁷⁹ V. Buescher,²⁴ V. Bunichev,³⁷ S. Burdin^b,⁴² T.H. Burnett,⁸⁰ C.P. Buszello,⁴¹ B. Calpas,¹⁵
11 E. Camacho-Pérez,³² M.A. Carrasco-Lizarraga,⁵⁶ B.C.K. Casey,⁴⁸ H. Castilla-Valdez,³² S. Chakrabarti,⁷⁰
12 D. Chakraborty,⁵⁰ K.M. Chan,⁵⁴ A. Chandra,⁷⁸ G. Chen,⁵⁶ S. Chevalier-Théry,¹⁸ D.K. Cho,⁷⁵ S.W. Cho,³¹
13 S. Choi,³¹ B. Choudhary,²⁸ T. Christoudias,⁴³ S. Cihangir,⁴⁸ D. Claes,⁶⁴ J. Clutter,⁵⁶ M. Cooke,⁴⁸ W.E. Cooper,⁴⁸
14 M. Corcoran,⁷⁸ F. Couderc,¹⁸ M.-C. Cousinou,¹⁵ A. Croc,¹⁸ D. Cutts,⁷⁵ A. Das,⁴⁵ G. Davies,⁴³ K. De,⁷⁶
15 S.J. de Jong,³⁴ E. De La Cruz-Burelo,³² F. Déliot,¹⁸ M. Demarteau,⁴⁸ R. Demina,⁶⁹ D. Denisov,⁴⁸ S.P. Denisov,³⁸
16 S. Desai,⁴⁸ K. DeVaughan,⁶⁴ H.T. Diehl,⁴⁸ M. Diesburg,⁴⁸ A. Dominguez,⁶⁴ T. Dorland,⁸⁰ A. Dubey,²⁸
17 L.V. Dudko,³⁷ D. Duggan,⁶⁵ A. Duperrin,¹⁵ S. Dutt,²⁷ A. Dyshkant,⁵⁰ M. Eads,⁶⁴ D. Edmunds,⁶² J. Ellison,⁴⁶
18 V.D. Elvira,⁴⁸ Y. Enari,¹⁷ H. Evans,⁵² A. Evdokimov,⁷¹ V.N. Evdokimov,³⁸ G. Facini,⁶⁰ T. Ferbel,⁶⁹ F. Fiedler,²⁴
19 F. Filthaut,³⁴ W. Fisher,⁶² H.E. Fisk,⁴⁸ M. Fortner,⁵⁰ H. Fox,⁴² S. Fuess,⁴⁸ T. Gadfort,⁷¹ A. Garcia-Bellido,⁶⁹

20 V. Gavrilov,³⁶ P. Gay,¹³ W. Geist,¹⁹ W. Geng,^{15,62} D. Gerbaudo,⁶⁶ C.E. Gerber,⁴⁹ Y. Gershtein,⁶⁵ G. Ginther,^{48,69}
 21 G. Golovanov,³⁵ A. Goussiou,⁸⁰ P.D. Grannis,⁷⁰ S. Greder,¹⁹ H. Greenlee,⁴⁸ Z.D. Greenwood,⁵⁸ E.M. Gregores,⁴
 22 G. Grenier,²⁰ Ph. Gris,¹³ J.-F. Grivaz,¹⁶ A. Grohsjean,¹⁸ S. Grünendahl,⁴⁸ M.W. Grünewald,³⁰ T. Guillemin,¹⁶
 23 F. Guo,⁷⁰ G. Gutierrez,⁴⁸ P. Gutierrez,⁷³ A. Haas^c,⁶⁸ S. Hagopian,⁴⁷ J. Haley,⁶⁰ L. Han,⁷ K. Harder,⁴⁴ A. Harel,⁶⁹
 24 J.M. Hauptman,⁵⁵ J. Hays,⁴³ T. Head,⁴⁴ T. Hebbeker,²¹ D. Hedin,⁵⁰ H. Hegab,⁷⁴ A.P. Heinson,⁴⁶ U. Heintz,⁷⁵
 25 C. Hensel,²³ I. Heredia-De La Cruz,³² K. Herner,⁶¹ G. Hesketh^d,⁴⁴ M.D. Hildreth,⁵⁴ R. Hirosky,⁷⁹ T. Hoang,⁴⁷
 26 J.D. Hobbs,⁷⁰ B. Hoeneisen,¹² M. Hohlfeld,²⁴ Z. Hubacek,^{10,18} N. Huske,¹⁷ V. Hynek,¹⁰ I. Iashvili,⁶⁷
 27 R. Illingworth,⁴⁸ A.S. Ito,⁴⁸ S. Jabeen,⁷⁵ M. Jaffré,¹⁶ D. Jamin,¹⁵ A. Jayasinghe,⁷³ R. Jesik,⁴³ K. Johns,⁴⁵
 28 M. Johnson,⁴⁸ D. Johnston,⁶⁴ A. Jonckheere,⁴⁸ P. Jonsson,⁴³ J. Joshi,²⁷ A. Juste,⁴⁰ K. Kaadze,⁵⁷ E. Kajfasz,¹⁵
 29 D. Karmanov,³⁷ P.A. Kasper,⁴⁸ I. Katsanos,⁶⁴ R. Kehoe,⁷⁷ S. Kermiche,¹⁵ N. Khalatyan,⁴⁸ A. Khanov,⁷⁴
 30 A. Kharchilava,⁶⁷ Y.N. Kharzheev,³⁵ D. Khatidze,⁷⁵ M.H. Kirby,⁵¹ J.M. Kohli,²⁷ A.V. Kozelov,³⁸ J. Kraus,⁶²
 31 S. Kulikov,³⁸ A. Kumar,⁶⁷ A. Kupco,¹¹ T. Kurča,²⁰ V.A. Kuzmin,³⁷ J. Kvita,⁹ S. Lammers,⁵² G. Landsberg,⁷⁵
 32 P. Lebrun,²⁰ H.S. Lee,³¹ S.W. Lee,⁵⁵ W.M. Lee,⁴⁸ J. Lellouch,¹⁷ L. Li,⁴⁶ Q.Z. Li,⁴⁸ S.M. Lietti,⁵ J.K. Lim,³¹
 33 D. Lincoln,⁴⁸ J. Linnemann,⁶² V.V. Lipaev,³⁸ R. Lipton,⁴⁸ Y. Liu,⁷ Z. Liu,⁶ A. Lobodenko,³⁹ M. Lokajicek,¹¹
 34 R. Lopes de Sa,⁷⁰ H.J. Lubatti,⁸⁰ R. Luna-Garcia^e,³² A.L. Lyon,⁴⁸ A.K.A. Maciel,² D. Mackin,⁷⁸ R. Madar,¹⁸
 35 R. Magaña-Villalba,³² S. Malik,⁶⁴ V.L. Malyshev,³⁵ Y. Maravin,⁵⁷ J. Martínez-Ortega,³² R. McCarthy,⁷⁰
 36 C.L. McGivern,⁵⁶ M.M. Meijer,³⁴ A. Melnitchouk,⁶³ D. Menezes,⁵⁰ P.G. Mercadante,⁴ M. Merkin,³⁷ A. Meyer,²¹
 37 J. Meyer,²³ F. Miconi,¹⁹ N.K. Mondal,²⁹ G.S. Muanza,¹⁵ M. Mulhearn,⁷⁹ E. Nagy,¹⁵ M. Naimuddin,²⁸ M. Narain,⁷⁵
 38 R. Nayyar,²⁸ H.A. Neal,⁶¹ J.P. Negret,⁸ P. Neustroev,³⁹ S.F. Novaes,⁵ T. Nunnemann,²⁵ G. Obrant,³⁹ J. Orduna,⁷⁸
 39 N. Osman,¹⁵ J. Osta,⁵⁴ G.J. Otero y Garzón,¹ M. Padilla,⁴⁶ A. Pal,⁷⁶ M. Pangilinan,⁷⁵ N. Parashar,⁵³
 40 V. Parihar,⁷⁵ S.K. Park,³¹ J. Parsons,⁶⁸ R. Partridge^c,⁷⁵ N. Parua,⁵² A. Patwa,⁷¹ B. Penning,⁴⁸ M. Perfilov,³⁷
 41 K. Peters,⁴⁴ Y. Peters,⁴⁴ K. Petridis,⁴⁴ G. Petrillo,⁶⁹ P. Pétrouff,¹⁶ R. Piegaiia,¹ J. Piper,⁶² M.-A. Pleier,⁷¹
 42 P.L.M. Podesta-Lerma^f,³² V.M. Podstavkov,⁴⁸ M.-E. Pol,² P. Polozov,³⁶ A.V. Popov,³⁸ M. Prewitt,⁷⁸ D. Price,⁵²
 43 N. Prokopenko,³⁸ S. Protopopescu,⁷¹ J. Qian,⁶¹ A. Quadt,²³ B. Quinn,⁶³ M.S. Rangel,² K. Ranjan,²⁸ P.N. Ratoff,⁴²
 44 I. Razumov,³⁸ P. Renkel,⁷⁷ M. Rijssenbeek,⁷⁰ I. Ripp-Baudot,¹⁹ F. Rizatdinova,⁷⁴ M. Rominsky,⁴⁸ A. Ross,⁴²
 45 C. Royon,¹⁸ P. Rubinov,⁴⁸ R. Ruchti,⁵⁴ G. Safronov,³⁶ G. Sajot,¹⁴ P. Salcido,⁵⁰ A. Sánchez-Hernández,³²
 46 M.P. Sanders,²⁵ B. Sanghi,⁴⁸ A.S. Santos,⁵ G. Savage,⁴⁸ L. Sawyer,⁵⁸ T. Scanlon,⁴³ R.D. Schamberger,⁷⁰
 47 Y. Scheglov,³⁹ H. Schellman,⁵¹ T. Schliephake,²⁶ S. Schlobohm,⁸⁰ C. Schwanenberger,⁴⁴ R. Schwienhorst,⁶²

48 J. Sekaric,⁵⁶ H. Severini,⁷³ E. Shabalina,²³ V. Shary,¹⁸ A.A. Shchukin,³⁸ R.K. Shivpuri,²⁸ V. Simak,¹⁰
 49 V. Sirotenko,⁴⁸ P. Skubic,⁷³ P. Slattery,⁶⁹ D. Smirnov,⁵⁴ K.J. Smith,⁶⁷ G.R. Snow,⁶⁴ J. Snow,⁷² S. Snyder,⁷¹
 50 S. Söldner-Rembold,⁴⁴ L. Sonnenschein,²¹ K. Soustruznik,⁹ J. Stark,¹⁴ V. Stolin,³⁶ D.A. Stoyanova,³⁸ M. Strauss,⁷³
 51 D. Strom,⁴⁹ L. Stutte,⁴⁸ L. Suter,⁴⁴ P. Svoisky,⁷³ M. Takahashi,⁴⁴ A. Tanasijczuk,¹ W. Taylor,⁶ M. Titov,¹⁸
 52 V.V. Tokmenin,³⁵ Y.-T. Tsai,⁶⁹ D. Tsybychev,⁷⁰ B. Tuchming,¹⁸ C. Tully,⁶⁶ P.M. Tuts,⁶⁸ L. Uvarov,³⁹ S. Uvarov,³⁹
 53 S. Uzunyan,⁵⁰ R. Van Kooten,⁵² W.M. van Leeuwen,³³ N. Varelas,⁴⁹ E.W. Varnes,⁴⁵ I.A. Vasilyev,³⁸ P. Verdier,²⁰
 54 L.S. Vertogradov,³⁵ M. Verzocchi,⁴⁸ M. Vesterinen,⁴⁴ D. Vilanova,¹⁸ P. Vint,⁴³ P. Vokac,¹⁰ H.D. Wahl,⁴⁷
 55 M.H.L.S. Wang,⁶⁹ J. Warchol,⁵⁴ G. Watts,⁸⁰ M. Wayne,⁵⁴ M. Weber,^{9,48} L. Welty-Rieger,⁵¹ A. White,⁷⁶ D. Wicke,²⁶
 56 M.R.J. Williams,⁴² G.W. Wilson,⁵⁶ M. Wobisch,⁵⁸ D.R. Wood,⁶⁰ T.R. Wyatt,⁴⁴ Y. Xie,⁴⁸ C. Xu,⁶¹ S. Yacoob,⁵¹
 57 R. Yamada,⁴⁸ W.-C. Yang,⁴⁴ T. Yasuda,⁴⁸ Y.A. Yatsunenko,³⁵ Z. Ye,⁴⁸ H. Yin,⁴⁸ K. Yip,⁷¹ S.W. Youn,⁴⁸
 58 J. Yu,⁷⁶ S. Zelitch,⁷⁹ T. Zhao,⁸⁰ B. Zhou,⁶¹ J. Zhu,⁶¹ M. Zielinski,⁶⁹ D. Zieminska,⁵² and L. Zivkovic⁷⁵

(The D0 Collaboration*)

¹*Universidad de Buenos Aires, Buenos Aires, Argentina*

²*LAFEX, Centro Brasileiro de Pesquisas Físicas, Rio de Janeiro, Brazil*

³*Universidade do Estado do Rio de Janeiro, Rio de Janeiro, Brazil*

⁴*Universidade Federal do ABC, Santo André, Brazil*

⁵*Instituto de Física Teórica, Universidade Estadual Paulista, São Paulo, Brazil*

⁶*Simon Fraser University, Vancouver, British Columbia, and York University, Toronto, Ontario, Canada*

⁷*University of Science and Technology of China, Hefei, People's Republic of China*

⁸*Universidad de los Andes, Bogotá, Colombia*

⁹*Charles University, Faculty of Mathematics and Physics,*

Center for Particle Physics, Prague, Czech Republic

¹⁰*Czech Technical University in Prague, Prague, Czech Republic*

¹¹*Center for Particle Physics, Institute of Physics,*

Academy of Sciences of the Czech Republic, Prague, Czech Republic

¹²*Universidad San Francisco de Quito, Quito, Ecuador*

¹³*LPC, Université Blaise Pascal, CNRS/IN2P3, Clermont, France*

¹⁴*LPSC, Université Joseph Fourier Grenoble 1, CNRS/IN2P3,*

Institut National Polytechnique de Grenoble, Grenoble, France

¹⁵*CPPM, Aix-Marseille Université, CNRS/IN2P3, Marseille, France*

* with visitors from ^aAugustana College, Sioux Falls, SD, USA, ^bThe University of Liverpool, Liverpool, UK, ^cSLAC, Menlo Park, CA, USA, ^dUniversity College London, London, UK, ^eCentro de Investigacion en Computacion - IPN, Mexico City, Mexico, ^fEFCM, Universidad Autonoma de Sinaloa, Culiacán, Mexico, and ^gUniversität Bern, Bern, Switzerland.

- 78 ¹⁶LAL, Université Paris-Sud, CNRS/IN2P3, Orsay, France
- 79 ¹⁷LPNHE, Universités Paris VI and VII, CNRS/IN2P3, Paris, France
- 80 ¹⁸CEA, Irfu, SPP, Saclay, France
- 81 ¹⁹IPHC, Université de Strasbourg, CNRS/IN2P3, Strasbourg, France
- 82 ²⁰IPNL, Université Lyon 1, CNRS/IN2P3, Villeurbanne, France and Université de Lyon, Lyon, France
- 83 ²¹III. Physikalisches Institut A, RWTH Aachen University, Aachen, Germany
- 84 ²²Physikalisches Institut, Universität Freiburg, Freiburg, Germany
- 85 ²³II. Physikalisches Institut, Georg-August-Universität Göttingen, Göttingen, Germany
- 86 ²⁴Institut für Physik, Universität Mainz, Mainz, Germany
- 87 ²⁵Ludwig-Maximilians-Universität München, München, Germany
- 88 ²⁶Fachbereich Physik, Bergische Universität Wuppertal, Wuppertal, Germany
- 89 ²⁷Panjab University, Chandigarh, India
- 90 ²⁸Delhi University, Delhi, India
- 91 ²⁹Tata Institute of Fundamental Research, Mumbai, India
- 92 ³⁰University College Dublin, Dublin, Ireland
- 93 ³¹Korea Detector Laboratory, Korea University, Seoul, Korea
- 94 ³²CINVESTAV, Mexico City, Mexico
- 95 ³³FOM-Institute NIKHEF and University of Amsterdam/NIKHEF, Amsterdam, The Netherlands
- 96 ³⁴Radboud University Nijmegen/NIKHEF, Nijmegen, The Netherlands
- 97 ³⁵Joint Institute for Nuclear Research, Dubna, Russia
- 98 ³⁶Institute for Theoretical and Experimental Physics, Moscow, Russia
- 99 ³⁷Moscow State University, Moscow, Russia
- 100 ³⁸Institute for High Energy Physics, Protvino, Russia
- 101 ³⁹Petersburg Nuclear Physics Institute, St. Petersburg, Russia
- 102 ⁴⁰Institució Catalana de Recerca i Estudis Avançats (ICREA) and Institut de Física d'Altes Energies (IFAE), Barcelona, Spain
- 103 ⁴¹Stockholm University, Stockholm and Uppsala University, Uppsala, Sweden
- 104 ⁴²Lancaster University, Lancaster LA1 4YB, United Kingdom
- 105 ⁴³Imperial College London, London SW7 2AZ, United Kingdom
- 106 ⁴⁴The University of Manchester, Manchester M13 9PL, United Kingdom
- 107 ⁴⁵University of Arizona, Tucson, Arizona 85721, USA
- 108 ⁴⁶University of California Riverside, Riverside, California 92521, USA
- 109 ⁴⁷Florida State University, Tallahassee, Florida 32306, USA

- 110 ⁴⁸*Fermi National Accelerator Laboratory, Batavia, Illinois 60510, USA*
- 111 ⁴⁹*University of Illinois at Chicago, Chicago, Illinois 60607, USA*
- 112 ⁵⁰*Northern Illinois University, DeKalb, Illinois 60115, USA*
- 113 ⁵¹*Northwestern University, Evanston, Illinois 60208, USA*
- 114 ⁵²*Indiana University, Bloomington, Indiana 47405, USA*
- 115 ⁵³*Purdue University Calumet, Hammond, Indiana 46323, USA*
- 116 ⁵⁴*University of Notre Dame, Notre Dame, Indiana 46556, USA*
- 117 ⁵⁵*Iowa State University, Ames, Iowa 50011, USA*
- 118 ⁵⁶*University of Kansas, Lawrence, Kansas 66045, USA*
- 119 ⁵⁷*Kansas State University, Manhattan, Kansas 66506, USA*
- 120 ⁵⁸*Louisiana Tech University, Ruston, Louisiana 71272, USA*
- 121 ⁵⁹*Boston University, Boston, Massachusetts 02215, USA*
- 122 ⁶⁰*Northeastern University, Boston, Massachusetts 02115, USA*
- 123 ⁶¹*University of Michigan, Ann Arbor, Michigan 48109, USA*
- 124 ⁶²*Michigan State University, East Lansing, Michigan 48824, USA*
- 125 ⁶³*University of Mississippi, University, Mississippi 38677, USA*
- 126 ⁶⁴*University of Nebraska, Lincoln, Nebraska 68588, USA*
- 127 ⁶⁵*Rutgers University, Piscataway, New Jersey 08855, USA*
- 128 ⁶⁶*Princeton University, Princeton, New Jersey 08544, USA*
- 129 ⁶⁷*State University of New York, Buffalo, New York 14260, USA*
- 130 ⁶⁸*Columbia University, New York, New York 10027, USA*
- 131 ⁶⁹*University of Rochester, Rochester, New York 14627, USA*
- 132 ⁷⁰*State University of New York, Stony Brook, New York 11794, USA*
- 133 ⁷¹*Brookhaven National Laboratory, Upton, New York 11973, USA*
- 134 ⁷²*Langston University, Langston, Oklahoma 73050, USA*
- 135 ⁷³*University of Oklahoma, Norman, Oklahoma 73019, USA*
- 136 ⁷⁴*Oklahoma State University, Stillwater, Oklahoma 74078, USA*
- 137 ⁷⁵*Brown University, Providence, Rhode Island 02912, USA*
- 138 ⁷⁶*University of Texas, Arlington, Texas 76019, USA*
- 139 ⁷⁷*Southern Methodist University, Dallas, Texas 75275, USA*
- 140 ⁷⁸*Rice University, Houston, Texas 77005, USA*
- 141 ⁷⁹*University of Virginia, Charlottesville, Virginia 22901, USA*

⁸⁰University of Washington, Seattle, Washington 98195, USA

We present a measurement of the top quark-antiquark pair production cross section in $p\bar{p}$ collisions at $\sqrt{s} = 1.96$ TeV using 5.4 fb^{-1} of data collected with the D0 detector. We consider decay channels with two electrons, two muons or one electron and one muon in the final state. For a top quark mass of $m_t = 172.5$ GeV, the measured cross section is $7.4^{+0.9}_{-0.8}$ (stat + syst) pb. This result combined with the cross section measurement in the lepton + jets final state yields a cross section of 7.6 ± 0.6 (stat + syst) pb which agrees with the standard model expectation.

PACS numbers: 14.65.Ha, 13.85.Lg, 13.85.Qk, 14.60Fg, 12.15.Ff

I. INTRODUCTION

Precisely measuring the top quark pair ($t\bar{t}$) production cross section ($\sigma_{t\bar{t}}$) and comparing such a measurement with the current predictions from the standard model (SM) provides an important test of perturbative Quantum Chromodynamics (QCD). At present, the most precise predictions of $\sigma_{t\bar{t}}$ are given by approximate next to next to leading order (NNLO) calculations [1–3] with a precision of 6% to 9% which challenge the experimental precision for the measurement of $\sigma_{t\bar{t}}$. Furthermore, because $\sigma_{t\bar{t}}$ depends on the top quark mass (m_t), it can be used to constrain that SM parameter [4, 5]. Comparing the SM prediction with the measured $\sigma_{t\bar{t}}$ value allows to test the presence of the physics beyond the SM, as for instance, scenarios in which the top quark would decay into a charged Higgs boson and a b quark [5].

In this letter we present an updated measurement of $\sigma_{t\bar{t}}$ in $p\bar{p}$ collisions at $\sqrt{s} = 1.96$ TeV in the dilepton ($\ell\bar{\ell}$) channel. In this channel both W bosons from top quark decay leptonically into $e\nu_e$, $\mu\nu_\mu$ or $\tau\nu_\tau$. We consider only $\tau \rightarrow e\nu_e\nu_\tau$, $\tau \rightarrow \mu\nu_\mu\nu_\tau$ decays, thus giving rise to the ee , $\mu\mu$ or $e\mu$ final states. This measurement complements the $\sigma_{t\bar{t}}$ measurements in the lepton+jets (ℓj) channel in which one of the W bosons from the top quark decays hadronically into a $q\bar{q}'$ pair and the other W boson decays leptonically [6, 7] as well as measurements in the all hadronic channel in which both W bosons decay hadronically [8].

The measurement is based on data collected with the D0 detector during Run II of the Fermilab Tevatron collider that correspond to an integrated luminosity of $5.4 \pm 0.3 \text{ fb}^{-1}$. This result supersedes our previous measurement [9], which used a dataset five times smaller than the one considered here. The CDF collaboration has performed a $\sigma_{t\bar{t}}$ measurement in the $\ell\ell$ channel using 2.8 fb^{-1} [10]. The ATLAS and CMS collaborations recently published their first $\sigma_{t\bar{t}}$ measurements in pp collisions at $\sqrt{s} = 7$ TeV [11, 12].

164 The D0 detector is described in detail in [13]. The region of the D0 detector closest to the interaction point contains
 165 a tracking system consisting of a silicon microstrip tracker (SMT) and a central fiber tracker (CFT) both located
 166 inside a superconducting solenoid magnet which generates a magnetic field of 1.9T. Hits in these two detectors are
 167 used to reconstruct tracks from charged particles in the pseudorapidity region $|\eta| < 3$ [28]. Surrounding the two
 168 tracking subdetectors are liquid argon-uranium calorimeters, segmented into electromagnetic and hadronic sections.
 169 The central section of the calorimeter (CC) covers pseudorapidities $|\eta| < 1.1$, and the two end calorimeters (EC)
 170 extend coverage to $|\eta| \approx 4.2$ with all three housed in separate cryostats. The muon system surrounds the calorimeter
 171 and consists of three layers of tracking detectors and scintillator trigger counters covering $|\eta| < 2$. A toroidal iron
 172 magnet with a field of 1.8T is located outside the innermost layer of the muon detector. The luminosity is calculated
 173 from the rate of inelastic $p\bar{p}$ collisions measured with plastic scintillator arrays, located in front of the EC cryostats [14].

174 The D0 trigger is based on a three-level pipeline system. The first level is implemented in custom-designed hardware.
 175 The second level uses high-level processors to combine information from the different sub-detectors to construct simple
 176 physics objects. The software-based third level uses full event information obtained with a simplified reconstruction
 177 algorithm.

178 II. OBJECT IDENTIFICATION

179 The $t\bar{t}$ dilepton final state contains two leptons (electrons or muons), at least two jets and significant transverse
 180 missing momentum.

181 Electrons are identified as energy clusters with radius $R = \sqrt{\Delta\eta^2 + \Delta\phi^2} < 0.2$ in the calorimeter consistent in their
 182 profile with an electromagnetic shower. More than 90% of the energy of the electron candidate should be deposited
 183 in the electromagnetic part of the calorimeter and it should have less than 20% of its energy in a calorimeter annulus
 184 of $0.2 < R < 0.4$ around its direction. This cluster has to be matched to a track. We consider electrons in CC
 185 with $|\eta| < 1.1$ and in EC with $1.5 < |\eta| < 2.5$. Additionally, we require an electron likelihood discriminant based on
 186 tracking and calorimeter information to be larger than 0.85.

187 A muon is identified as a segment in at least one layer of the outer muon chambers in the full acceptance of the D0
 188 muon system, matched to a track in the central tracking system. Reconstructed muons should satisfy two isolation
 189 criteria. First, the transverse energy deposit in a calorimeter annulus around the muon $0.1 < R < 0.4$ ($E_T^{\mu \text{ iso}}$) has
 190 to be smaller than 15% of the transverse momentum of the muon (p_T^μ). Second, the sum of the p_T of the tracks in a
 191 cone of radius $R < 0.5$ around the muon track in the central tracking system ($p_T^{\mu \text{ iso}}$) has to be smaller than 15%

192 of p_T^μ . Muons that fulfill these isolation criteria are referred to as tight isolated muons.

193 For events simulated with Monte Carlo (MC) the residual differences with data in the electron or muon p_T resolution
 194 and in the electron or muon identification efficiencies are corrected. These corrections are derived by measuring the
 195 efficiencies and resolutions in $Z/\gamma^* \rightarrow \ell\ell$ data and MC events, identifying one tight lepton as tag and using the other
 196 charged lepton as a probe (tag-and-probe method).

197 Jets are identified with a fixed cone algorithm with radius $R < 0.5$ [15]. We consider jets in the range $|\eta| < 2.5$. A
 198 jet energy scale correction (JES) is determined by calibrating the energy deposited in the jet cone using transverse
 199 momentum balance in γ +jet and dijet events. If a muon overlaps with the jet cone, the momentum of that muon is
 200 included in the correction to account for the energy lost to semileptonic hadron decays.

201 We require that the jets are matched to at least two tracks originating from the vertex of the primary interaction
 202 (PV). Jets in MC are corrected for the residual difference between data and MC in the energy resolution and JES.
 203 These correction factors are measured by comparing data and MC in $(Z/\gamma^* \rightarrow ee)$ +jets events.

204 We use a neural-network (NN) tagging algorithm [16] to identify jets from b quarks. The algorithm combines
 205 information from the impact parameter of the tracks and variables that characterize the presence and properties of
 206 secondary vertices within the jet. In order to use this information for b -tagging, the jet is required to be matched to
 207 a jet built from tracks. Jets fulfilling this requirement are called taggable jets.

208 The missing transverse momentum (\cancel{p}_T) is reconstructed from the energy deposited in the calorimeter cells. Cor-
 209 rection for lepton and jet p_T 's are propagated into the \cancel{p}_T . The missing transverse momentum significance ($\sigma_{\cancel{p}_T}$) is
 210 defined in each event as \cancel{p}_T divided by its uncertainty.

211 More details about object identification can be found in [17].

212 III. EVENT SELECTION AND BACKGROUND ESTIMATION

213 The main sources of background in the $\ell\ell$ channel come from Drell-Yan and Z boson production ($Z/\gamma^* \rightarrow \ell\ell$),
 214 diboson production (WW, WZ, ZZ) and instrumental background. The instrumental background mainly arises from
 215 multijet and W +jets events in which one or two jets are misidentified as electrons or an isolated muon originating of
 216 semileptonic decays of a heavy flavor quark is emitted by jet.

217 For this analysis we consider events that fired a set of single lepton triggers for the ee and $\mu\mu$ channels. For the $e\mu$
 218 channel we consider events selected by any trigger. Efficiencies for single lepton triggers have been measured using
 219 the tag-and-probe method with $Z/\gamma^* \rightarrow \ell\ell$ data. These efficiencies are found to be around 99% for the ee channel and

220 80% for the $\mu\mu$ final state. For the $e\mu$ channel the overall efficiency of the single lepton and electron-muon triggers is
 221 close to 100%.

222 In order to separate the $t\bar{t}$ signal events from background, the following selection is applied:

- 223 • We require at least one PV in the beam interaction region with $|Z| < 60$ cm, where Z is the coordinate along
 224 the beam axis and $Z=0$ in the center of the detector. At least three tracks must be associated with this PV.
- 225 • We require at least two isolated leptons with transverse momentum $p_T > 15$ GeV. These two leptons must
 226 originate from the same PV, i.e. the difference between the Z coordinates of the two lepton tracks should be less
 227 than 2 cm, where the Z coordinate is calculated at the point of the track closest approach to the beam.
- 228 • We require the two selected leptons to have opposite charge.
- 229 • In the $e\mu$ final state we require the distance between the electron and the muon directions: $R(e, \mu) > 0.3$ to
 230 reduce the background from bremsstrahlung.
- 231 • We require at least two jets with $p_T > 20$ GeV. In the $e\mu$ channel, we also consider events with only one jet.
- 232 • To further improve the signal purity of the selected sample, we apply additional topological selections. In the
 233 $e\mu$ final state with two jets we require $H_T > 110$ GeV, where H_T is the scalar sum of the transverse momenta of
 234 the leading lepton and the two leading jets. In the $e\mu$ channel with exactly one jet we require $H_T > 105$ GeV.
 235 In the ee final state, we require $\sigma_{p_T} > 5$ while in the $\mu\mu$ channel we require that $\cancel{p}_T > 40$ GeV and $\sigma_{p_T} > 5$.

236 In order to estimate the signal efficiency and the background contamination we use the MC simulation for all
 237 contributions but the instrumental background, the latter being derived with data. The $t\bar{t}$ and Z/γ^* events are
 238 generated with the tree level matrix element generator ALPGEN [18] interfaced with the PYTHIA [19] generator for
 239 parton showering and hadronization. Diboson events are generated with PYTHIA. All simulated samples are generated
 240 using the CTEQ6L1 parton distribution functions (PDFs) [20]. The Z/γ^* samples are normalized to the NNLO cross
 241 section computed for different dilepton invariant mass ranges with the FEWZ program [21]. We simulate separately
 242 Z/γ^* with heavy flavor (HF) quarks Z/γ^*+bb (or Z/γ^*+cc) using ALPGEN and enhance the corresponding leading
 243 order cross sections by a factor of 1.5 (1.7) estimated with the MCFM program [22]. The diboson samples are
 244 normalized to the next to leading order cross section calculated with MCFM. Uncertainties in these normalization
 245 factors are taken into account as systematic uncertainties. We additionally apply a correction to the Z/γ^*+jets
 246 simulation to address the imperfect modeling of the Z boson p_T in the MC.

247 The instrumental background is estimated directly from data. First, in the ee and $e\mu$ channels we determine the
 248 contribution of events with jets misidentified as electrons using the signal data sample but without electron likelihood

TABLE I: Numbers of expected and observed events assuming the SM $t\bar{t}$ cross section for a top mass of $m_t = 172.5$ GeV (7.45 pb). The expected number of events is shown with its systematic uncertainties. The uncertainty on the ratio between observed and expected number of events takes into account the statistical uncertainty in the observed number of events and the systematic uncertainty in the expected number of events.

Channel	$Z \rightarrow \ell\ell$	Diboson	Instrumental background	$t\bar{t} \rightarrow \ell\bar{\ell}b\bar{b}\nu\bar{\nu}$	Expected N of events	Observed N of events	$\frac{Observed}{Expected}$
$e\mu$ two jets	30.3 ± 4.2	8.6 ± 1.2	22.7 ± 8.6	191.5 ± 18.8	253.1 ± 24.3	281	1.11 ± 0.13
$e\mu$ one jet	40.9 ± 4.8	20.7 ± 2.4	25.3 ± 10.5	52.1 ± 9.4	139.0 ± 16.5	150	1.08 ± 0.16
ee	12.6 ± 2.0	3.0 ± 0.4	-	45.6 ± 5.3	61.1 ± 7.1	74	1.21 ± 0.20
$\mu\mu$	67.3 ± 9.7	5.1 ± 0.7	7.6 ± 1.2	59.8 ± 6.6	139.8 ± 15.7	144	1.03 ± 0.14

discriminant cut. We extract the number of events with misidentified jets, n_f , and the number of events with real electrons, n_e , by fitting the electron likelihood distribution with an extended likelihood fit, using the following likelihood function:

$$\mathcal{L} = \prod_{i=1}^N [n_e S(x_i) + n_f B(x_i)] \frac{e^{-n_e+n_f}}{N!}, \quad (1)$$

where N is the number of selected events and $S(x_i)$ and $B(x_i)$ are the signal and background probability density functions (pdf), and i runs over all selected events. The signal pdf is measured in $Z/\gamma^* \rightarrow ee$ data events. The background pdf is measured in $e\mu$ events with the same selection as the analysis sample but inverting the opposite sign lepton requirement (same sign sample) without any topological requirement but with muon anti-isolation cuts: $E_T^{\mu iso}/p_T^\mu > 0.2$ and $p_T^{\mu iso}/p_T^\mu > 0.2$. The total number of events with a jet misidentified as an electron in the signal selection can be found as $n = n_f \int_{0.85}^{1.0} B(x) dx$, where the integration is done over the high likelihood region. The estimation is performed separately in CC and EC. It was found that the contribution of instrumental background to the ee channel is negligible.

In a second step, we determine the number of events with an isolated muon arising from jets in the $e\mu$ and $\mu\mu$ channels. This number is estimated as $n_f^\mu = N_{loose} f_\mu$, where N_{loose} is the number of events in the same sign sample with loose isolation criteria on the muon: $E_T^{\mu iso}/p_T^\mu < 0.5$ and $p_T^{\mu iso}/p_T^\mu < 0.5$. In the $\mu\mu$ final state we apply these loose isolation cuts only to one randomly chosen muon. In the $e\mu$ channel, the number of events with jets misidentified as electrons in the same sign sample is subtracted from N_{loose} . The muon fake isolation rate f_μ is determined in a dimuon sample with at least one jet. In this sample we require one muon to be close to the jet ($dR(\mu, jet) < 0.5$) with anti-isolation cuts $E_T^{\mu iso}/p_T^\mu > 0.15$ and $p_T^{\mu iso}/p_T^\mu > 0.15$. The other muon defined as the probe should pass the loose isolation cuts $E_T^{\mu iso}/p_T^\mu < 0.5$ and $p_T^{\mu iso}/p_T^\mu < 0.5$. We compute f_μ as the ratio of the number of events in which the probe muon passes the tight isolation cuts to the total number of events in this same-sign sample.

269 The number of predicted background events as well as the expected number of signal events in the different channels
 270 are shown in Table I. In order to achieve a better separation between signal and background when measuring the
 271 cross section we use the distribution of the smallest of the two b -tagging NN discriminant outputs of the two leading
 272 jets. These NN discriminant distributions for the different channels are shown in Fig. 1. We measure the $t\bar{t}$ cross
 273 section $\sigma_{t\bar{t}}$ by simultaneously fitting the NN distributions in the four channels and maximizing the following likelihood
 274 function:

$$\mathcal{L} = \prod_{i=1}^{i \leq 4} \prod_{j=1}^{j \leq 14} P(n_{ij}, \mu_{ij}(\sigma_{t\bar{t}})), \quad (2)$$

275 where i runs over the channels and j over the bins of the NN distribution, $P(n, \mu(\sigma_{t\bar{t}}))$ is the Poisson probability
 276 function to observe n events when $\mu(\sigma_{t\bar{t}})$ events are expected.

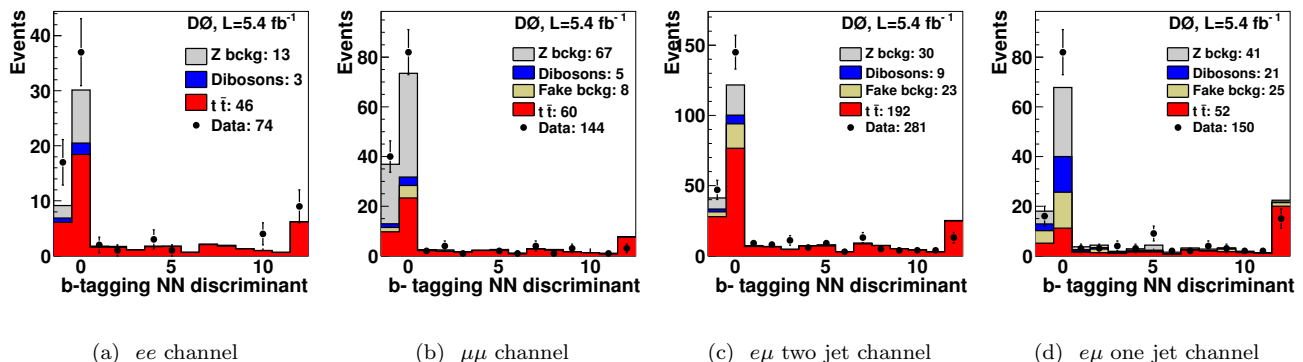


FIG. 1: Expected and observed distributions for the smallest b -tagging NN discriminant outputs of the two leading jets. The $t\bar{t}$ signal is normalized to the SM cross section (7.45 pb). The X axis represents the NN output non-uniformly mapped to 14 bins. The bin with central value 0 represents the lowest probability for a jet to be produced by a b quark. The bin with value 12 represents the highest probability. The bin with value -1 represents the jets which do not satisfy the requirements to enter to the NN computation (non-taggable jets).

IV. RESULTS AND UNCERTAINTIES

277

278 The main systematic uncertainties for the measurement of the $t\bar{t}$ cross section are described in the following. The
 279 uncertainty in the measured integrated luminosity of 6.1% [14] affects directly the cross section measurement, but
 280 also the expected number of Z/γ^* and diboson background events. Uncertainties in lepton identification efficiencies
 281 are determined by evaluating the different sources of bias in the tag-and-probe method and data/MC differences in
 282 $Z/\gamma^* \rightarrow \ell\ell$ events. Uncertainties in the lepton energy resolution are determined by comparing the width of the Z
 283 boson invariant mass distribution in data and MC.

284 The uncertainty in the relative JES between data and MC for light quark jets is measured in Z/γ^* +jets events.
 285 The uncertainty on the difference between light and b quark JES (1.8%) is estimated by propagating the difference
 286 in the single pion response between data and MC to the MC JES for b quark jets. Jet energy resolution uncertainties
 287 are estimated by comparing the resolution measured in Z/γ^* +jets events in data and MC. The uncertainty on the
 288 jet identification efficiency is estimated by comparing the efficiency measured in dijet events for data and MC. The b
 289 quark identification uncertainties include uncertainties in the probability to tag a b quark jet, the probability to tag
 290 a light quark jet or gluon and the probability for a jet not to be taggable [16].

291 To estimate the uncertainty in the trigger efficiency we use events selected with the same criteria as the $t\bar{t}$ signal
 292 but without any jet requirement. In all the channels this selection is dominated by Z/γ^* events. We compute the
 293 ratio of the expected and observed number of events for two cases: when both leptons are allowed to fire the trigger
 294 or when only one lepton is allowed to fire the trigger. The difference in these ratios is used to estimate the uncertainty
 295 on the trigger efficiency.

296 Several uncertainties on the signal modeling are considered. The effects of higher order corrections and the
 297 hadronization modeling have been estimated as the difference in signal efficiency using the default ALPGEN+ PYTHIA
 298 simulation and using events generated with the MC@NLO [23] generator. The uncertainty coming from color recon-
 299 nection is evaluated by comparing the $t\bar{t}$ efficiency using PYTHIA v6.4 tune Apro and PYTHIA v6.4 tune ACRpro [24].
 300 The uncertainty on initial (ISR) and final (FSR) state radiation is evaluated by varying the ISR/FSR parameters in
 301 PYTHIA, and evaluating the change in the signal efficiency. The uncertainty due to PDFs is estimated by reweighting
 302 the signal efficiency to CTEQ6.1M [25] and looking at the efficiency variation along the 20 CTEQ6.1M eigenvector
 303 errors. The uncertainty due to the simulation of b quark fragmentation is assigned as the difference between tuning
 304 the parameters of the b quark fragmentation function to LEP or SLD data [26].

305 The uncertainty in the background normalization includes the theoretical uncertainties in the cross section and the
 306 uncertainty due to the correction for the Z boson p_T modeling. We also take into account an uncertainty due to
 307 the limited statistics of the signal and background templates of the NN discriminant. For the following systematic
 308 uncertainties we take into account the shape changing effects of the b -tagging NN output discriminant: jet energy
 309 scale, jet resolution, jet identification and b quark identification uncertainties.

310 Maximizing the likelihood function (2) and using the above systematic uncertainties, we measure the $t\bar{t}$ cross section

311 for a top quark mass of $m_t = 172.5$ GeV and we find:

$$\sigma_{t\bar{t}} = 8.0 \pm 0.5 \text{ (stat)} \pm 1.0 \text{ (syst)} \text{ pb.} \quad (3)$$

312 In order to reduce the influence of systematic uncertainties on the cross section measurement we use the nuisance
 313 parameters technique [27] to constrain the overall uncertainty using the data NN output distribution itself. Using
 314 this technique the likelihood (2) has to be modified to be:

$$\mathcal{L} = \prod_{i=1}^{i \leq 4} \prod_{j=1}^{j \leq 14} P(n_{ij}, \mu_{ij}(\sigma_{t\bar{t}})) \prod_k \mathcal{G}(\nu_k; 0, SD). \quad (4)$$

315 The impact of each uncertainty k is parameterized by a nuisance parameter ν_k that is constrained with a Gaussian
 316 probability \mathcal{G} with a mean of zero and a width corresponding to the size (SD) of the uncertainty. Correlations of
 317 systematic uncertainties between channels and between the different samples are naturally taken into account by
 318 assigning the same nuisance parameter to the correlated systematic uncertainty. In formula (4), the free parameters
 319 of the fit are ν_k and $\sigma_{t\bar{t}}$.

320 As can be seen from (3), the systematic uncertainties are the limiting uncertainties in the precision of the $t\bar{t}$ cross
 321 section measurement. Varying the systematic uncertainties and constraining them with data using the nuisance
 322 parameter technique can therefore significantly improve the measurement. Using the nuisance parameter technique
 323 we find an improved overall uncertainty of approximately 20% and reach a relative precision of 11% in the $t\bar{t}$ cross
 324 section:

$$\sigma_{t\bar{t}} = 7.4_{-0.8}^{+0.9} \text{ (stat + syst)} \text{ pb}$$

325 for $m_t = 172.5$ GeV. The uncertainties in this measurement are summarized in Table II. For each category of
 326 systematic uncertainties listed in Table II, only the corresponding nuisance parameters are allowed to vary. The
 327 absolute shift of the measured $t\bar{t}$ cross section with respect to the result obtained including only statistical uncertainties
 328 is shown in the column “Offset”. In the columns “+ σ ” and “- σ ” the systematic uncertainty on the measured cross
 329 section for each category are listed. The line “Fit result” contains the result of the full nuisance parameter fit, where
 330 all nuisance parameters are allowed to vary at the same time, which can result in a different “offset” and different
 331 uncertainties in the final $t\bar{t}$ cross section than expected from the sum of the individual “offsets” and systematic

332 uncertainties. The uncertainty quoted in this line includes the full statistical and systematic uncertainty on the
 333 result.

TABLE II: Measured $t\bar{t}$ cross section with the breakdown of uncertainties in the $\ell\ell$ channel and for the combined $\ell\ell$ and ℓj measurement using the nuisance parameter technique. The offsets show how the mean value of the measured cross section is shifted due to each source of systematic uncertainty. In each line, all but the considered source of systematic uncertainty are ignored. The $\pm\sigma$ give the impact on the measured cross section when the nuisance parameters describing the considered category are changed by ± 1 SD of their fitted value. See text for further details.

Source	$\ell\ell$				$\ell\ell+\ell j$				
	$\sigma_{t\bar{t}}$ [pb]	Offset [pb]	$+\sigma$ [pb]	$-\sigma$ [pb]	$\sigma_{t\bar{t}}$ [pb]	Offset [pb]	$+\sigma$ [pb]	$-\sigma$ [pb]	
Statistical only		+8.04	+0.50	-0.48	+7.72		+0.20	-0.20	
Muon identification		+0.00	+0.13	-0.12		-0.06	+0.06	-0.06	
Electron identification and smearing		-0.22	+0.28	-0.25		+0.05	+0.13	-0.13	
Signal modeling		+0.05	+0.39	-0.34		-0.04	+0.17	-0.15	
Triggers		-0.01	+0.07	-0.07		-0.10	+0.10	-0.10	
Jet energy scale		-0.16	+0.16	-0.15		-0.01	+0.03	-0.03	
Jet reconstruction and identification		-0.21	+0.24	-0.22		+0.24	+0.08	-0.08	
b-tagging		+0.14	+0.00	+0.00		-0.04	+0.16	-0.12	
Background normalization		-0.27	+0.27	-0.25		-0.07	+0.11	-0.11	
Instrumental background		-0.08	+0.19	-0.19		-0.01	+0.05	-0.05	
Luminosity		-0.66	+0.59	-0.51		-0.43	+0.45	-0.40	
Other		-0.04	+0.12	-0.11		-0.50	+0.58	+0.52	
Template statistics		+0.00	+0.09	+0.09		+0.00	0.04	-0.04	
Total systematics			-1.46	+0.89	+0.80		-0.50	+0.58	+0.52
Fit result	7.42		+0.90	-0.79	7.61		+0.63	-0.57	

334 Furthermore, we combine this measurement with the cross section measurement in the fully orthogonal ℓj channel [6]
 335 using the same nuisance parameter approach and taking all correlations into account. In the ℓj channel the events
 336 are separated into events with three or at least four jets, of which zero, one or at least two jets are b -tagged. In
 337 events that have three or four jets but no b -tagged jets or events with three jets and one b -tagged jet, we use a
 338 topological discriminant to improve the separation of signal and background. In Ref. [6] the separation into these
 339 channels and application of topological methods is referred to as the combined method. For this combination, we did
 340 not simultaneously fit the heavy flavor fraction for W +jet processes (W +HF) in the ℓj channel as was done in Ref. [6],
 341 making it unnecessary to use ℓj events with only two jets. With this change compared to Ref. [6] the measured ℓj $t\bar{t}$
 342 cross section for $m_t = 172.5$ GeV is:

$$\sigma_{t\bar{t}} = 7.9^{+0.8}_{-0.7} (\text{stat} + \text{syst}) \text{ pb.}$$

343 The combination of the measurements in the ℓj and $\ell\ell$ final states is done by maximizing the product of the

344 likelihood function for dilepton (2) and the likelihood function of the ℓj channel [6], which yields:

$$\sigma_{t\bar{t}} = 7.6 \pm 0.6 \text{ (stat + syst) pb}$$

345 for $m_t = 172.5$ GeV. This combination has a relative precision of 8% and represents an improvement of about 12%
 346 relative to the ℓj cross section measurement alone. The uncertainties for this combined measurement are summarized
 347 in Table II.

348 Due to acceptance effects, the $t\bar{t}$ efficiency depends on the assumed top quark mass in the MC. We extract the $t\bar{t}$
 349 cross sections using simulated $t\bar{t}$ events with different values of m_t . The resulting cross sections can be fitted with the
 350 following functional form:

$$\begin{aligned} \sigma_{t\bar{t}}(m_t) = & \frac{1}{m_t^4} [a + b(m_t - 170 \text{ GeV}) \\ & + c(m_t - 170 \text{ GeV})^2 + d(m_t - 170 \text{ GeV})^3] \text{ pb,} \end{aligned} \quad (5)$$

351 with $a = 6.57141 \times 10^9 \text{ GeV}^4$, $b = 7.96467 \times 10^7 \text{ GeV}^3$, $c = 9.30737 \times 10^5 \text{ GeV}^2$ and $d = -2.770 \times 10^3 \text{ GeV}$ and where
 352 $\sigma_{t\bar{t}}$ and m_t are in pb and GeV respectively. Figure 2 shows this parameterization for the measurement as a function
 353 of top quark mass together with approximate NNLO computations [1–3].

354 V. CONCLUSION

355 In this letter we presented an updated measurement of the $t\bar{t}$ production cross section in the dilepton final state
 356 using 5.4 fb^{-1} of data. This cross section measurement yields $7.4_{-0.8}^{+0.9}$ (stat + syst) pb and has a relative precision of
 357 $\begin{smallmatrix} +12\% \\ -11\% \end{smallmatrix}$. It is currently the most precise measurement of the $t\bar{t}$ cross section in the dilepton channel. Combining the
 358 measurement in the dilepton channel with the result in the lepton + jets channel [6] yields 7.6 ± 0.6 (stat + syst) pb
 359 which corresponds to a relative precision of 8%. This measurement is in good agreement with the SM prediction.

360 We thank the staffs at Fermilab and collaborating institutions, and acknowledge support from the DOE and
 361 NSF (USA); CEA and CNRS/IN2P3 (France); FASI, Rosatom and RFBR (Russia); CNPq, FAPERJ, FAPESP and
 362 FUNDUNESP (Brazil); DAE and DST (India); Colciencias (Colombia); CONACyT (Mexico); KRF and KOSEF
 363 (Korea); CONICET and UBACyT (Argentina); FOM (The Netherlands); STFC and the Royal Society (United
 364 Kingdom); MSMT and GACR (Czech Republic); CRC Program and NSERC (Canada); BMBF and DFG (Germany);

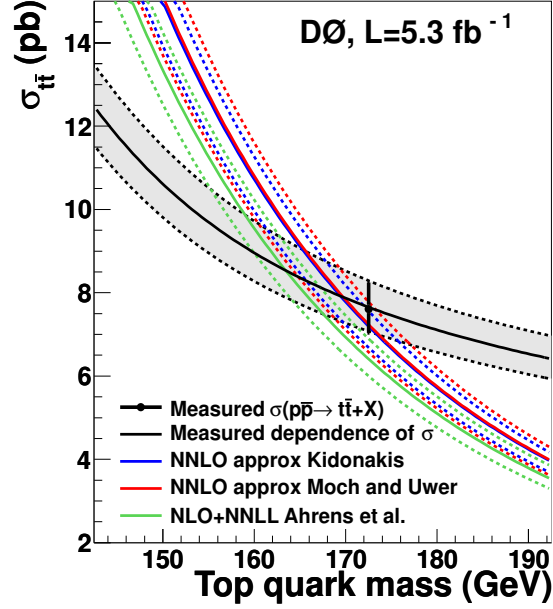


FIG. 2: Dependence of the experimental and theoretical [1–3] $t\bar{t}$ cross sections on the top quark mass. The point shows the combined $\ell\ell$ and ℓj cross section measurement for $m_t = 172.5$ GeV.

365 SFI (Ireland); The Swedish Research Council (Sweden); and CAS and CNSF (China).

-
- 366 [1] V. Ahrens, A. Ferroglia, M. Neubert, B. D. Pecjak, and L. L. Yang, *J. High Energy Phys.* **1009**, 097 (2010); V. Ahrens,
 367 A. Ferroglia, M. Neubert, B. D. Pecjak, and L. L. Yang, *Nucl. Phys. Proc. Suppl.* **205–206**, 48 (2010).
- 368 [2] S. Moch and P. Uwer, *PRD* **78**, 034003 (2008); U. Langenfeld, S. Moch, and P. Uwer, *PRD* **80**, 054009 (2009).
- 369 [3] N. Kidonakis and R. Vogt, *PRD* **68**, 114014 (2003); N. Kidonakis, *PRD* **82**, 114030 (2010).
- 370 [4] V. M. Abazov *et al.* (D0 Collaboration), *Phys. Lett. B* **679**, 177 (2009).
- 371 [5] V. M. Abazov *et al.* (D0 Collaboration), *Phys. Rev. D* **80**, 071102 (2009).
- 372 [6] V. M. Abazov *et al.* (D0 Collaboration), arXiv:1101.0124.
- 373 [7] V. M. Abazov *et al.* (D0 Collaboration), *Phys. Rev. Lett.* **100**, 192004 (2008).
- 374 [8] V. M. Abazov *et al.* (D0 Collaboration), *Phys. Rev. D* **76**, 072007 (2007); V. M. Abazov *et al.* (D0 Collaboration),
 375 *Phys. Rev. D* **82**, 032002 (2010).
- 376 [9] V. M. Abazov *et al.* (D0 Collaboration), *Phys. Lett. B* **626**, 55 (2005).
- 377 [10] T. Aaltonen *et al.* (CDF Collaboration), *Phys. Rev. D* **82**, 052002 (2010).
- 378 [11] G. Aad *et al.* (ATLAS Collaboration), arXiv:1012.1792.
- 379 [12] V. Khachatryan *et al.* (CMS Collaboration), *Phys. Lett. B* **695**, 424 (2011).

- 380 [13] V. M. Abazov *et al.* (D0 Collaboration), Nucl. Instrum. Methods Phys. Res. A **565**, 463 (2006).
- 381 [14] T. Andeen *et al.*, FERMILAB-TM-2365 (2007).
- 382 [15] G. C. Blazey *et al.*, in *Proceedings of the Workshop: "QCD and Weak Boson Physics in Run II,"* edited by U. Baur,
383 R. K. Ellis, and D. Zeppenfeld (Fermilab, Batavia, IL, 2000) p. 47; see Sec. 3.5 for details.
- 384 [16] V. M. Abazov *et al.* (D0 Collaboration) Nucl. Instrum. Methods Phys. Res. A **620**, 490 (2010).
- 385 [17] V. M. Abazov *et al.* (D0 Collaboration), Phys. Rev. D **76**, 052006 (2007).
- 386 [18] M. L. Mangano, M. Moretti, F. Piccinini, R. Pittau, and A. D. Polosa, J. High Energy Phys. **0307**, 001 (2003).
- 387 [19] T. Sjostrand, S. Mrenna, and P. Z. Skands, J. High Energy Phys. **0605**, 026 (2006).
- 388 [20] J. Pumplin *et al.*, (CTEQ Collaboration), J. High Energy Phys. **07**, 012 (2002).
- 389 [21] R. Gavin, Y. Li, F. Petriello and S. Quackenbush, arXiv:1011.3540 [hep-ph].
- 390 [22] R. K. Ellis, Nucl. Phys. Proc. Suppl. **160**, 170 (2006).
- 391 [23] S. Frixione and B. R. Webber, arXiv:hep-ph/0612272.
- 392 [24] A. Buckley, H. Hoeth, H. Lacker, H. Schulz and J. E. von Seggern, Eur. Phys. J. C **65**, 331 (2010);
393 P. Z. Skands and D. Wicke, Eur. Phys. J. C **52**, 133 (2007).
- 394 [25] P. M. Nadolsky *et al.*, Phys. Rev. D **78**, 013004 (2008).
- 395 [26] Y. Peters, K. Hamacher and D. Wicke, FERMILAB-TM-2425-E.
- 396 [27] P. Sinervo, *In the Proceedings of PHYSTAT2003: Statistical Problems in Particle Physics, Astrophysics, and Cosmology,*
397 *Menlo Park, California, 8-11 Sep 2003, pp TUAT004.*
- 398 [28] The pseudorapidity is defined as $\eta = -\ln[\tan(\theta/2)]$, where θ is the polar angle with respect to the proton beam.